NASA Final report for proposal NAG5-7295

Coronal Reconstruction using LASCO and UVCS Observations

Principal Investigator: P. P. Hick

1. Introduction

The main goal of the research described in the original proposal was to develop methods to quantify coronal and inner-heliospheric velocity fields of the 'quiet' solar wind. For this we planned to use several sources of observations:

- SOHO/UVCS velocity information in the range 1.5–3 $R_\odot$ obtained from Doppler dimming observations.
- projected solar wind velocities (into the plane of the sky) obtained from SOHO/ LASCO images (1.1–30 $R_\odot$), primarily derived from two-dimensional correlation tracking techniques.
- Interplanetary scintillation observations of the heliospheric (> 26 $R_\odot$) solar wind velocity from the Solar-Terrestrial Environment Laboratory (STELab) in Nagoya, Japan.
- *Ecliptic in situ observations*: data for the ecliptic solar wind are available from the MIT and Los Alamos plasma experiments on the Earth-orbiting IMP–8 spacecraft, from the Celias instrument on SOHO near the L1 Lagrange point, and from the WIND spacecraft.
- *Out-of-ecliptic in situ observations*: these data are available primarily from the Los Alamos SWOOPS instrument on Ulysses, which passed over the solar north pole in August 1995, about one year prior to the Whole Sun Month period.

Where ever possible we planned to use the first Whole Sun Month as the main time period for the analysis, since we expected that for this period it would be easiest to obtain adequate coverage over the extended period of time required to analyze 'quiet' solar wind patterns.

Beyond the observations mentioned above (primarily SOHO data) we extended our selection of data to several events identified in the Yohkoh/SXT data base which directly promised to provide us with clues about the connection between the slow solar wind observed by IPS in the inner heliosphere and their sources in the low corona, in particular active regions. We also obtained valuable results using SWOOPS *in situ* observations from the pole-to-pole passage of Ulysses in a comparison with solar wind velocities derived from a tomographic reconstruction of Nagoya IPS observations.

2. Principal Results

The principal successes of this research were obtained from a study of LASCO and IPS observations during the Whole Sun Month, from the comparison of Ulysses SWOOPS data with IPS observations and from the study of Yohkoh/SXT data and. These are discussed below in separate subsections.

Negative results need to be reported in two significant aspects of the study. We were not successful in matching UVCS Doppler dimming velocities with solar wind velocities from IPS tomography. In this analysis of images from the SOHO/UVCS instrument for the Whole Sun Month we did not find any convincing correspondence with solar wind velocities obtained using tomographic reconstruction from interplanetary scintillation data (see synoptic map in Figure 6). We also did not find a detailed correspondence with density enhancements detected in the LASCO images (we primarily looked at C3 images). We suspect that the main problem is associated with line-of-sight ambiguities in the UVCS velocities. For the IPS velocities the tomographic reconstruction is specifically designed to resolve these ambiguities, *i.e.* solar wind velocities are derived in a heliographic coordinate system (as in Figure 6). Probably a similar tomographic approach is needed to translate the (line-of-sight integrated) UVCS Doppler-dimming velocities into actual solar wind speeds as a function of heliographic location (similar to the IPS tomography). Only in this way may it be possible to make progress in understanding the UVCS data in relation to the solar wind velocities obtained from IPS tomography.

Attempts at a 2D-correlation analysis to determine outflow speeds from difference images of the LASCO C3 coronagraph were only marginally successful. In the case of the Whole Sun Month some indications of slow solar wind outflow, apparently associated with the main active region present during this period were observed. However, no systematic flow patterns sustained over longer periods of time (*i.e.* several days) could be identified. We suspect that part of this negative result is due to a limitation inherent in the LASCO C3 images. Our 2D-correlations suggest the presence of systematic noise sources of unknown origin (pixel-to-pixel variations, and maybe subpixel variationts, are potential candidates) which mask real outflow patterns to such an extent that a consistent 2D-correlation tracking of flow patterns in the solar wind through the C3 field of view (as opposed to tracking individual small-scale features as in Sheeley *et al.*, 1997) becomes uncertain at best. Progress in this area may depend on the availability of a flat-field correction (which to the best of our knowledge is not readily available). This aspect of the 2D-correlation tracking procedure is still under investigation.

2.1. Ulysses pole-to-pole passage in 1994/1995

Over the past few years we have developed a numerical technique for reconstructing the density and velocity distribution in the inner heliosphere from remote sensing observations (Jackson *et al.*, 1998). We used this technique in this project to analyze IPS observations from STELab in Nagoya, Japan (primarily IPS velocity data, but recently also *g*-level observations). The same approach can be applied to other heliospheric remote sensing observations. In particular Thomson scattering data can be used to replace

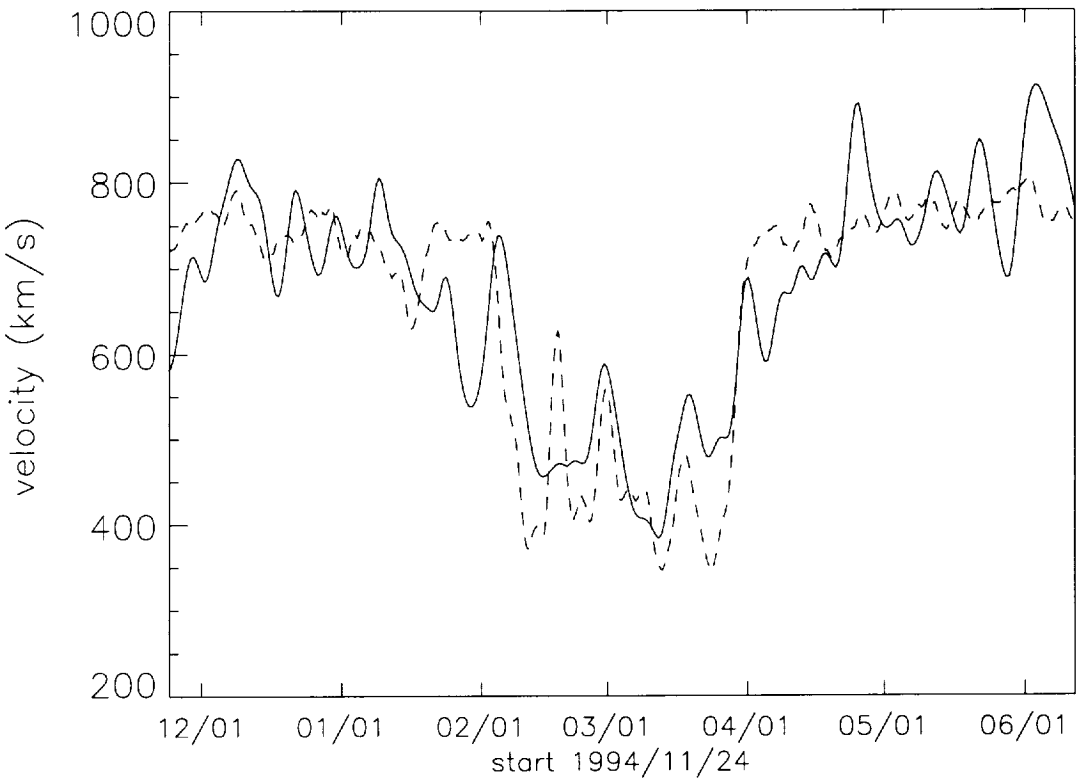

Figure 1. Comparison of time series of the solar wind velocity derived for a tomographic reconstruction of IPS velocity data (solid line) and *in situ* observations from the Ulysses/SWOOPS instrument (dashed line). The SWOOPS data are smoothed using a 3-day running mean. The time period covers the pole-to-pole passage of Ulysses. The tomographic time series was calculated using $\beta_n = 0.3$ and $\beta_r = 0.5$.

g-level data as a source of information about the solar wind density. For the analysis of IPS observations a central aspect is the relation between *g*-level and heliospheric density. This relation is expressed as an empirical power-law relation between the density fluctuations δn, the heliospheric distance r, and the normalized heliospheric density $\tilde{n}$ (*i.e.* density $\times r^2$), $\delta n = \delta n_0 (\tilde{n}/n_0)^{\beta_n} (r_0/r)^{2-\beta_r}$ (Hick and Jackson, 2000). The value for $\beta_n \approx 0.3$–0.5 is fairly well established from comparisons with *in situ* density observations from Earth orbit (primarily IMP-8; Tappin *et al.*, 1986, Jackson *et al.*, 1994). However, the value of β_r is less certain (values in the literature vary between 0 and 1; see *e.g.* Asai *et al.*, 1997). The power β_r primarily determines the velocity scale in the tomographic reconstruction. In the past, we tentatively attributed systematic deviations between tomographic velocities and *in situ* observations in the ecliptic to uncertainties in the value of β_r.

The Ulysses pole-to-pole passage in winter 1994/1995 provided us with a unique opportunity to 'calibrate' the velocity scale for tomographic IPS reconstructions. *In situ*

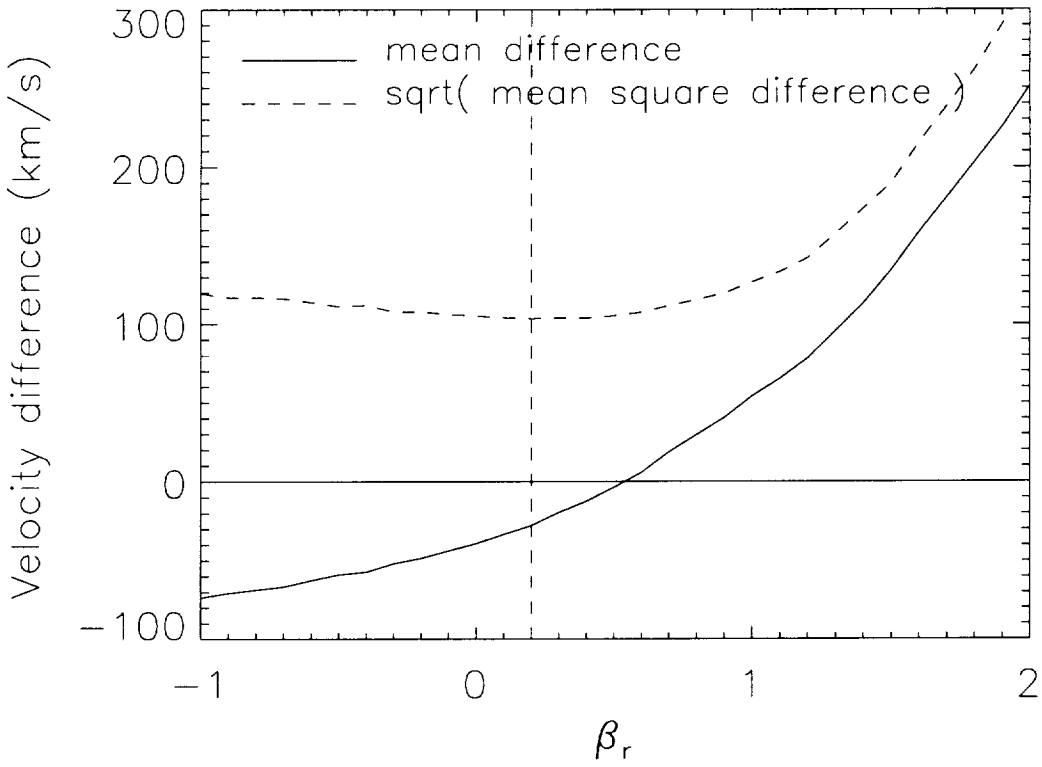

Figure 2. Mean difference and mean square difference of tomographic and SWOOPS velocity time series for the time period shown in Figure 1 as a function of β_r (with β_n = 0.3).

data from SWOOPS between November 1994 and June 1995 while Ulysses passed from heliographic latitude –70° to +70°, provide extensive coverage of both slow and fast solar wind (Figure 1, dashed curve). We applied our tomography technique to Nagoya IPS data from May-June 1995 (the IPS data closest to the time of the Ulysses flyby) for a range of values of β_r and compared this with the SWOOPS time series. The result is shown in Figure 2. A value of $\beta_r \approx 0.5$ minimizes the systematic difference between the SWOOPS *in situ* velocity and the IPS tomographic reconstruction over the latitude range –70° to +70°. The comparison of the best-fit tomographic and SWOOPS time series for the velocity is shown in Figure 1.

This result has significantly increased the reliability of the velocity reconstructions from the IPS velocity and *g*-level data, in particular at high heliographic latitudes (*i.e.* in the fast solar wind over the solar poles). This result is currently being prepared for publication as part of a paper on our tomographic technique for remote sensing observations (Hick and Jackson, 2000).

2.2. Slow solar wind observed after an eruptive SXT X-ray flare.

X-ray images from the Yohkoh/SXT instrument, obtained during and after limb flares sometimes show coronal fan-like structures extending above a growing post-flare loop system. The first such event identified by us occurred in active region AR 7270 on 28/29 August 1992, while the active region was on the east limb. This event was analyzed in detail, using a comparison of X-ray data with synoptic maps of the solar wind density, constructed from a tomographic analysis of interplanetary scintillation (IPS) *g*-level measurements, obtained with the IPS array in Cambridge (UK).

Figure 3 shows three *Yohkoh*/SXT images for the August 1992 event. There are several indications that this was an eruptive event, resulting in the opening of the active region magnetic field for a period of many hours. At 21:22 UT, 28 August (Figure 3a), an extensive rising arch-like structure was seen above the region. After the transit of the arch a dimming of the X-ray corona or 'cavity' was observed (Figure 3b), which is often associated with a CME (Hudson *et al.*, 1996). In *SGD* (1993), Holloman AFB reports an eruptive prominence at the limb in the position of AR 7270 starting at or before 21:34 UT. In all three images of Figure 3 a post-flare loop system can be seen at increasing coronal heights following the CME-related arch. Finally, GOES reported a long–duration X-ray event between 22:11 UT, 28 August, to 00:18 UT, 29 August.

Figure 3. *Yohkoh/SXT* images of active region AR 7270. Post-flare loops are seen at increasing heights in all three images. *(a)* (left) 21:22 UT, 28 August: an extensive arch, probably indicating the onset of a CME, is seen rising above the post-flare loops. *(b)* (center) 22:10 UT, 28 August: the region evacuated by the rising arch shows a significant dimming in soft X-rays. *(c)* (right) 02:43 UT, 29 August: a fan–like structure of rays extends above the post-flare loop system.

Presumably the CME associated with the arch-like structure removed all coronal material present above the active region. Then, during the rise of the flare loops, a new coronal configuration developed, resembling a fan of coronal rays embedded in a post–flare loop system (Figure 3c). The individual fan elements look like rays extending from the active region into the 'cavity' left by the CME. Since the active region magnetic field was

opened by the eruptive event it seems likely that the rays extended high enough to provide a direct connection with the solar wind.

We analyzed IPS *g*-level observations from Cambridge (UK), obtained at heliocentric distances between 0.5 and 1.0 AU for August/September 1992. Figure 4a shows a synoptic solar wind density map for parts of Carrington rotations 1859 and 1860, derived from these IPS data by tomographic reconstruction (Jackson *et al.*, 1998), and projected back to the solar surface assuming a radial outflow speed of 400 km s^{-1}. Active region AR 7270 is clearly identifiable as an enhanced density area. Figure 4b is based on the same IPS data, except for a 5-day period following the flare. The disappearance of the density enhancement when these 5 days are omitted indicates that the enhancement was limited to at most a few days following the occurrence of the eruptive flare. Hence the synoptic maps show enhanced scintillation matching the position of AR 7270 at a time consistent with the appearance of the fan-like X-ray structure.

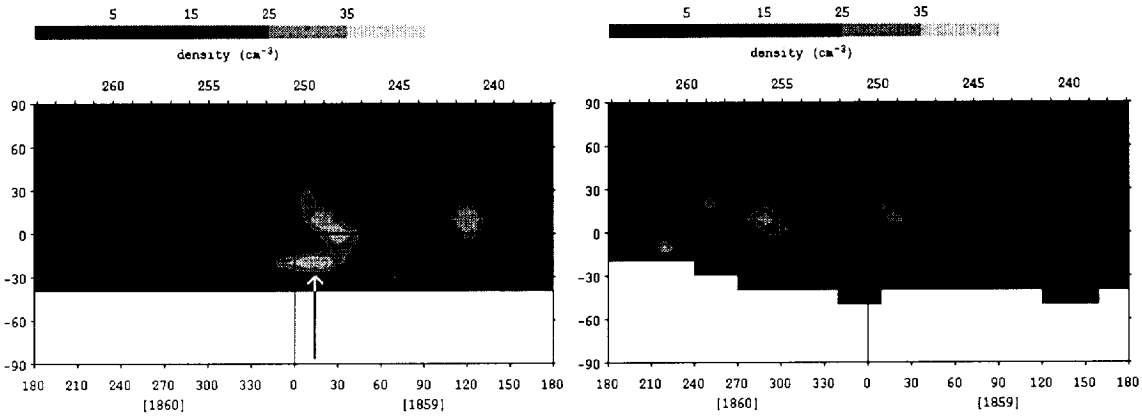

Figure 4. Solar wind density maps derived from a tomographic reconstruction of IPS *g*-factor observations, covering the period during which AR 7270 crossed the solar disk (rotations 1859 and 1860). *(a)* (left) Map based on all IPS data from mid-August to mid-September, 1992. The position of AR 7270 is marked with an arrow. *(b)* (right) Map for same data as (a) but with a 5–day period following the flare excluded.

From this agreement we argue that outflow of mass occurs from the active region into interplanetary space following the occurrence of many eruptive flares for a period of perhaps several days. We suggest that the rays in the X-ray fan are 'ministreamers', formed as a result of the re-structuring of the corona following the occurrence of a flare-associated CME. These results have been published in Hick *et al.* (1999) and Svestka *et al.* (1998).

Several similar events have been discovered in more recent SXT data. A particularly interesting event after a flare on 20 January 1999 is discussed by McKenzie and Hudson (1999). Unfortunately no SOHO or IPS data are available for this event. Currently we are looking for similar events for which simultaneous SOHO/LASCO, Yohkoh/SXT and Nagoya IPS data are available. This should enable a much more detailed analysis of the connection between X-ray fans and the slow solar wind.

2.3. Whole Sun Month: Comparison of densities and velocities using LASCO and Nagoya IPS data.

For the first Whole Sun Month period we studied the global density and velocity distribution from the solar surface out to 1 AU. As the main result of this study we showed that slow solar wind outflow patterns persist (at least) out to 1 AU. This is illustrated in Figure 5 through Figure 7. Figure 5 shows a synoptic emission density map based on LASCO C1 images. These images were processed using a tomographic reconstruction method developed by S. Zidowitz (1996, 1997). The map covers 360° in heliographic longitude (parts of Carrington rotation 1912 and 1913) corresponding to the Whole Sun Month period in 1996. The main high-density coronal feature in this period coincides with NOAA active region AR 7986 near heliographic latitude −15° and longitude ≈260°. The active region is the only significant high-density feature visible in the C1 synoptic map. The active region is also clearly visible in a synoptic map based on Mark III data (not shown here; see Web site http://www.hao.ucar.edu/public/research/mlso/data_archive.html).

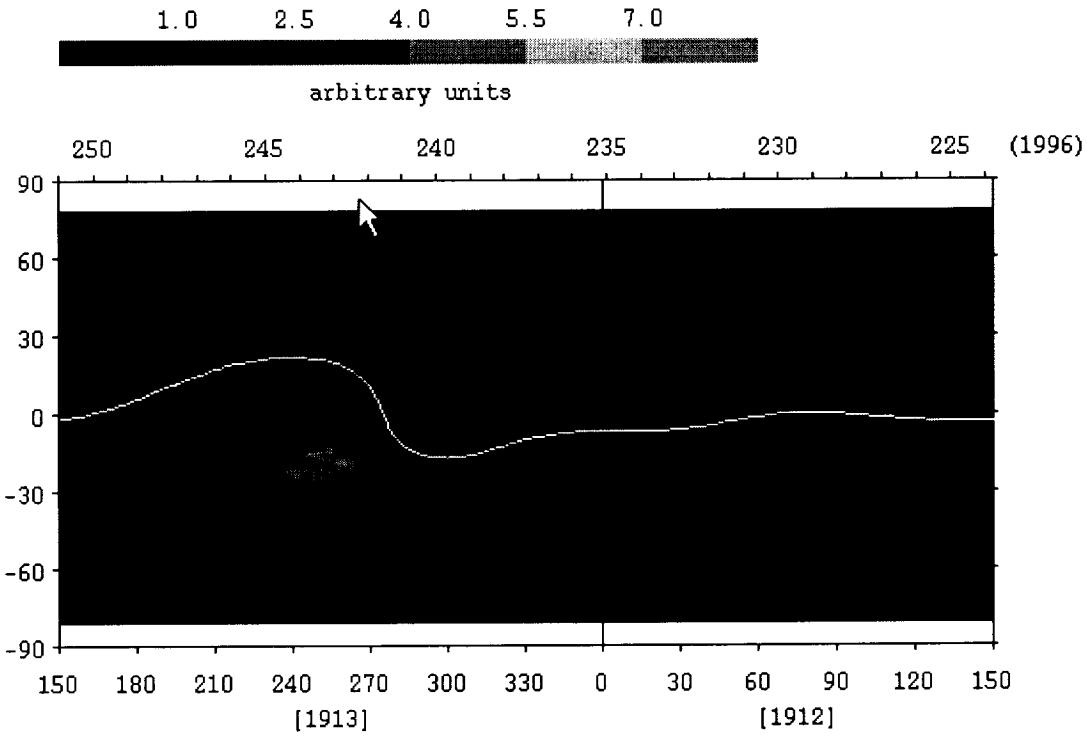

Figure 5. Synoptic map of coronal emission density (in arbitray units) at 1.2 $R_\odot$ derived from a tomographic construction (Zidowitz, 1996, 1997) based on LASCO C1 images during the Whole Sun Month (courtesy S. Zidowitz). The main feature (between longitudes 240° and 270° at latitude −15°) is associated with active region AR 7986. Overplotted is the Stanford heliospheric current sheet at 2.5 $R_\odot$.

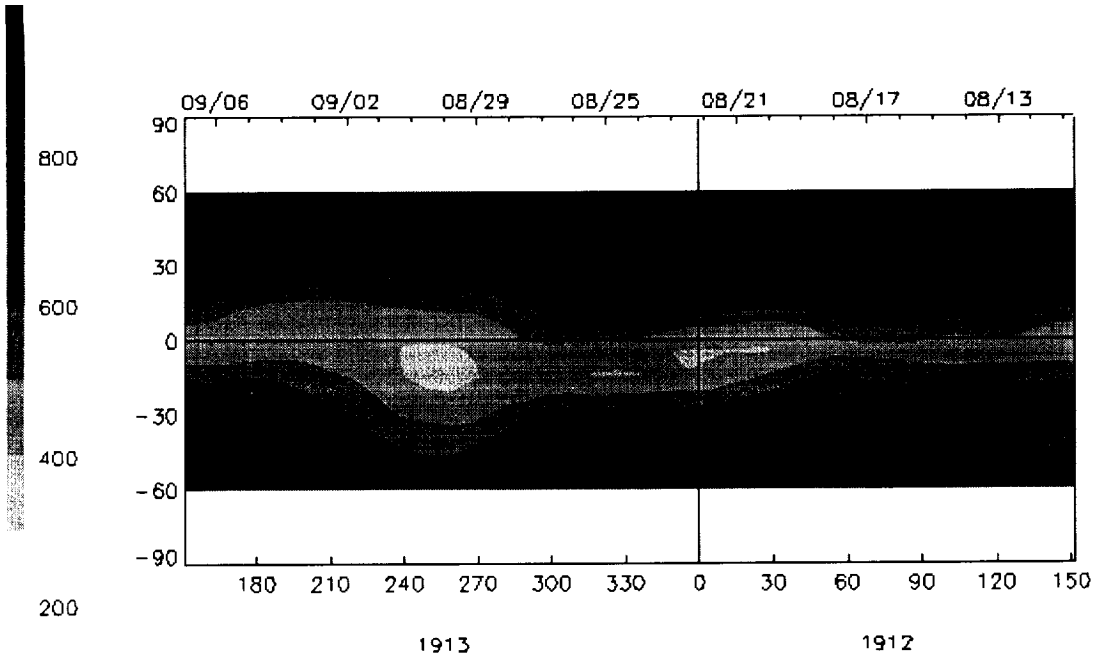

Figure 6. Velocity map at 2.5 $R_\odot$ derived from Nagoya IPS velocity data obtained during the Whole Sun Month. The map is derived from a 3D tomographic reconstruction of the solar wind velocity between 2.5 $R_\odot$ and 1.5 AU based on the IPS data. Clearly identifiable is a low velocity outflow pattern (V≈300 km/s) associated with active region 7986 between 240° and 270° longitude.

We applied our tomographic technique for remote sensing data (Jackson *et al.*, 1998; Hick and Jackson, 2000) to STELab IPS velocity data from August / September 1996 (covering the Whole Sun Month) to obtain the quiet component of the solar wind outflow. The tomography provides the three-dimensional solar wind velocity between the lower boundary (set to 2.5 $R_\odot$) and an outer boundary (set to 1.5 AU). The result at the lower boundary is shown in Figure 6. The velocity map shows a low velocity band which to a large extent follows the Stanford current sheet (white line in Figure 5). The main deviation from the current sheet occurs between heliographic longitudes 240° and 270°. Here a local minimum in the solar wind speed close to 300 km/s appears centered on heliographic latitude −10°, *i.e.* coinciding with the location of AR 7986. This strongly suggests that a persistent slow solar wind outflow pattern associated with the active region retains its identity throughout the heliospheric distance range where the IPS observations are obtained (*i.e.* at least out to 1 AU).

As a further confirmation that the slow solar wind outflow from the active region (located close to the ecliptic) persist out to 1 AU we checked *in situ* observations of the solar wind density and velocity from the WIND spacecraft (Figure 7). The top graph in Figure 7 shows the WIND observations for most of the Whole Sun Month period, plotting density and velocity as a function of the heliographic longitude of Earth.

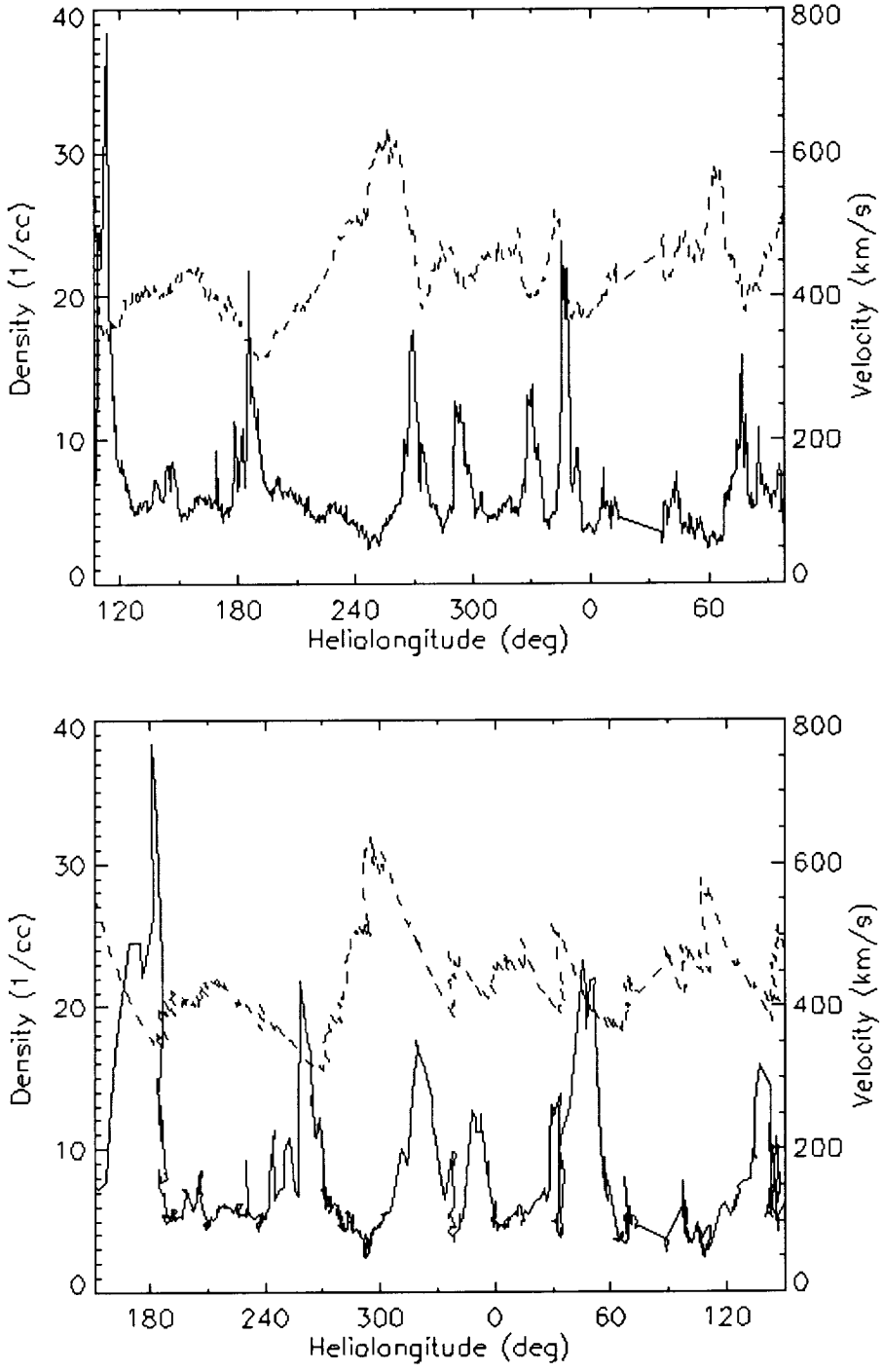

Figure 7. (top) WIND time series for density (solid) and velocity (dashed) during the Whole Sun Month (plotted as a function of the heliographic longitude of Earth. (bottom). Same WIND time series mapped back to the solar surface by a ballistic mapping using the WIND velocity. A low velocity, high density solar wind pattern between longitudes 240° and 270° corresponds with active region AR 7986.

The bottom graph shows the same data traced back to the solar surface using the WIND velocity in a ballistic mapping. This mapping approximately identifies the solar origin of the solar wind observed by WIND. Figure 7 shows that the low velocity (≈300 km/s), high density (≈20 cm^{-3}) peak observed by WIND while the spacecraft was between heliographic longitudes 180° and 200° (top graph in Figure 7) originated at the solar surface between longitudes 250° and 270°, consistent with the location of AR 7986.

It should be noted that this analysis was confirmed by Yokobe *et al.* (1999) using a different tomographic reconstruction method (Kojima *et al.*, 1997) based on the same data.

3. Publications

The following papers acknowledge this proposal: Hick *et al.* (1999), Svestka *et al.* (1998) and Hick and Jackson (2000).

4. References

Asai, K., Kojima, M., Tokumaru, M., Yokobe, A., Jackson, B.V. and Hick, P.L., 'Heliospheric tomography using interplanetary scintillation observations, 3. Correlation between speed and electron density fluctuations in the solar wind', *J. Geophys. Res.* **103 (A2)**, 1991–2001, 1997.

Hick, P., Svestka, Z., Jackson, B.V., Farnik, F. and Hudson, H., 'Quiet solar wind signatures above active regions observed in X-rays', in: *Solar Wind Nine*, SR. Habbal, R. Esser, J.V. Hollweg, P.A. Isenberg (eds.), p. 231, AIP Conf. Proc. 471, 1999.

Hick, P. P. and Jackson, B.V., 'A technique for tomographic reconstruction based on remote sensing observation', in preparation for submission to Solar Physics, 2000.

Hudson, H.S., Lemen, J.R. and Webb, D.F., 'Coronal X-ray dimming in two limb flares', in: *Magnetic Reconnection in the Solar Atmosphere*, R.D. Bentley and J.T. Mariska (eds.), *ASP Conf. Series* **111**, 379–382, 1996.

Jackson, B.V., Hick, P., Altrock, R.C., Woan, G. and Kojima, M., 'Velocity and Scintillation-Level IPS Carrington Synoptic Comparisons with Ulysses Polar Data', *EOS* **75 (44/Suppl.)**, 518, AGU Fall Meeting, San Francisco, 1994.

Jackson, B.V., Hick, P.L., Kojima, M. and Yokobe, A., 'Heliospheric Tomography Using Interplanetary Scintillation Observations, I. Combined Nagoya and Cambridge observations', *J. Geophys. Res.* **103 (A6)**, 12049–12067, 1998.

Kojima, M., Tokumaru, M., Watanabe, H., Yokobe, A., Jackson, B.V. and Hick, P.L., 'Heliospheric tomography using interplanetary scintillation observations, 2. Latitude and

heliocentric distance dependence of solar wind structure at 0.1–1 AU', *J. Geophys. Res.* **103 (A2)**, 1981–1989, 1997.

McKenzie, D.E. and Hudson, H.S., 'X-ray observations of motions and structure above a solar flare arcade', *Astrophys. J. Lett.* **519** (in press), 1999.

Sheeley, N.R., Y.-M. Wang, S.H. Hawley, G.E. Brueckner, K.P. Dere, R.A. Howard, M.J. Koomen, C.M. Korendyke, D.J. Michels, S.E. Paswaters, D.G. Socker, O.C. St. Cyr, D. Wang, P.L. Lamy, A. Llebaria, R. Schwenn, G.M. Simnett, S. Plunkett, D.A. Biesecker, 'Measurements of flow speeds in the corona between 2 and 30 Rs', *Astrophys. J.*, **484**, 472–478, 1997.

Svestka, Z., Farnik, F., Hudson, H.S. and Hick, P., 'Large-scale active coronal phenomena in Yohkoh SXT images, IV. Solar wind streams from flaring active regions', *Solar Phys.* **182**, 179–193, 1998.

Tappin, S.J., 'Interplanetary scintillation and plasma density', *Planetary Space Sci.* **34**, 93, 1986.

Yokobe, A., Ohmi, T., Hakamada, K., Kojima, M., Tokumaru, M., Jackson, B.V., Hick, P.P. and Zidowitz, S., 'Comparison of solar speed with coronagraph data analyzed by tomography', in: *Solar Wind Nine*, S.R. Habbal, R. Esser, J.V. Hollweg and P.A. Isenberg (eds.), pp. 565-567, AIP Conf. Proc. 471, Woodbury, New York, 1999.

Zidowitz, S, *Tomographische Inversion von Koronagraphen-Bildern*, Thesis, Technischen Universität Carolo-Wilhelmina zu Braunschweig, 1997.

Zidowitz, S., Inhester, B. and Epple, A., 'Tomographic inversion of coronagraph images', in: *Solar Wind Eight*, D. Winterhalter, J.T. Gosling, S.R. Habbal, W.S. Kurth and M. Neugebauer (ed.), pp. 165–166, AIP Conf. Proc. 328, Woodbury, New York, 1996.